J Oceanogr (2015) 71:251–262
DOI 10.1007/s10872-015-0282-8

ORIGINAL ARTICLE

Signatures of tidal interference patterns in the South China Sea

Alex Warn-Varnas[1,2] · Dong S. Ko[3] · Avijit Gangopadhyay[2]

Received: 25 June 2014 / Revised: 25 February 2015 / Accepted: 10 March 2015 / Published online: 22 March 2015

Abstract The formation of arc-type structures in the surface elevation and temperature fields due to internal tidal (IT) waves is studied in the region of the South China Sea (SCS) and Luzon Strait. It is demonstrated that these arc-type structures in the surface elevation and temperature at depth result from the merging of IT waves. Predictions of internal baroclinic tides are conducted with a nonlinear hydrostatic model, the Luzon Strait Nowcast/Forecast System, forced with tides, realistic surface forcing and stratification (Appendix 1). It is shown that IT waves generated by the undersea ridges near the Batan and Babuyan Islands in the Luzon Strait propagate westward and merge into arcs in the SCS. The superposition of IT waves is also investigated with a linear knife-edge model (Appendix 2). M_2 and K_1 tidal waves are considered. It is demonstrated that K_1, M_2 tidal waves from the Babuyan Islands combine with waves from the Batan Islands to form arc signatures in sea surface elevation and warm spots in the South China Sea. Possible modulation effects of K_1 waves on M_2 waves are shown. Dynamics of the nonlinear hydrostatic model shape the arc segments differently from the linear model. Arc lengths increase from the sources in nonlinear and linear models. The model-predicted merged IT waves are compared with SAR images.

Keywords Tidal interference pattern · South China Sea · Internal tide · Luzon Strait Nowcast/Forecast System (LZSNFS) · Linear knife-edge model

1 Introduction

Many recent experiments were conducted in the northern South China Sea (SCS) and Luzon Strait (LS) to investigate large-amplitude internal waves. Among these are the Asian Seas International Acoustics Experiment (ASIAEX-2001), the Windy Island Soliton Experiment/Variability in the northern South China Sea (WISE/VANS-2005), Nonlinear Internal Waves Initiative/South China Sea Ocean Prediction Experiment (NLIWI/SCOPE-2007), and the Internal Waves in Straits Experiment (IWISE-2011). These experiments, together with Synthetic Aperture Radar (SAR) satellite observations, have tracked internal tides (ITs) and internal solitary waves (ISWs) propagating from Luzon Strait to the west in the South China Sea.

Hsu and Liu (2000) compiled an internal wave distribution map from SAR images for the years 1993–1998. The map exhibits arc type signatures of internal waves west of the Luzon Strait. The arcs are short close to the strait and merge into larger arcs proceeding further west. Jackson (2009) compiled satellite images from April 2003 to December 2006. The resultant map (Fig. 1) indicates small arcs in the Luzon Strait combining into larger arcs proceeding west. Analysis of mooring data (Ramp et al. 2004, 2010) leads to a classification of ISWs into type A and type B. A-waves are larger and arrive in pairs of two diurnally. B-waves are smaller and arrive as a single wave between A-waves. The B-waves arrive about an hour later each day. A-waves propagate northwestward and B-waves southwestward from Luzon Strait into the SCS.

✉ Dong S. Ko
ko@nrlssc.navy.mil

[1] Jacobs Technologies Inc., Stennis Space Center, MS 39529, USA

[2] Department of Estuarine and Ocean Sciences, University of Massachusetts Dartmouth, Dartmouth, MA 02747, USA

[3] Naval Research Laboratory, Stennis Space Center, MS 39529, USA

There are several generation sites of ITs in the Luzon Strait. One is at the Batan Islands and another at the Babuyan Islands (Fig. 1). The generated IT waves propagate westwards with a surface elevation signature and warm water signature at depth. From the Babuyan Islands, A-waves have been observed to propagate northwestward along a direction of 282°, and from the Batan Islands, B-waves propagate along a more westerly direction of 267° (Ramp et al. 2004, 2010; Zhang et al. 2011).

Forecast models for the SCS and LS based on the Naval Coastal Ocean Model (NCOM), such as Luzon Strait Nowcast/Forecast System (LZSNFS; Chao et al. 2007; Qian et al. 2010; Simmons et al. 2011; Chen et al. 2013), provide information on generation sites of internal tides that evolve into ISWs. Depth integrated energy flux calculations from models over latitude and longitude in the SCS and LS region yield information on direction of energy flux flow (e.g., Niwa and Hibiya 2004; Chen et al. 2013). Directions of energy flux flow from the Batan and Babuyan Islands are traceable (e.g., Chao et al. 2007; Chen et al. 2013; Ma et al. 2013).

ISWs evolve on the leading edge of internal tidal depressions (ITDs). This has been demonstrated in the SCS with non hydrostatic 2D model simulations of ISWs, e.g., Warn-Varnas et al. (2010), and 3D simulations of ISWs, e.g., Zhang et al. (2011). Results of 3D simulations agreed with mooring data and satellite observations.

The hydrostatic prediction with LZSNFS provides the location where ISWs evolve from ITs as they propagate westward away from Luzon Strait. This has been verified through a comparison of LZSNFS predictions of internal tidal depressions in SCS with ship track observations of ISWs by Chao et al. (2007).

Our aim in this paper is to investigate the interference patterns of internal tides generated at the Batan and Babuyan Islands. We study propagation of diurnal and semidiurnal internal tides from these two source regions and the resultant arc type interference patterns in the SCS. Propagation of IT waves is simulated by applying the nonlinear hydrostatic model LZSNFS (described in Appendix 1) and a linear knife-edge model of St. Laurant et al. (2003) (described in Appendix 2). The model simulations and observational data are related to physical phenomena in SCS. The effects of parameter variations and physical phenomena representation are investigated.

The paper is structured as follows. SAR and in situ observations of IT and ISW frontal structure in the SCS are described in Sect. 2. The nonlinear hydrostatic model predictions in the SCS of merging IT waves, containing topography and mesoscale variability with Kuroshio, are presented in Sect. 3. The interference patterns predicted with a linear knife-edge model that demonstrates how much of the interference patterns a linear model can predict are described in Sect. 4. The discussion, considering the generation, propagation, interference patterns of internal tide waves (ITWs) from the Batan and Babuyan island chains, is presented in Sect. 5. A conclusion highlighting the results is given in Sect. 6. The nonlinear hydrostatic model and the linear knife-edge model are described in Appendices 1 and 2, respectively.

2 SAR and in situ observations of ISWs

Figure 1a and b shows SAR images of ISWs in the SCS, compiled from February 2003 through December 2006 (Jackson 2009, 2014). Figure 1a indicates A-waves and Fig. 1b indicates B-waves. The signatures are line and arc shapes, and are a composite in location and time. Coming out of Luzon Strait, there are small arc signatures of ISWs that have originated from the Batan and Babuyan Islands (Liu et al. 2004). As the waves propagate westward, they combine to form interference patterns of larger arc structures. These arc structures enlarge further with westward propagation.

Internal tidal depressions and internal solitary waves are related. Internal solitary waves evolve in the trough of ITDs. First one ISW evolves and then others can evolve. The ISWs are phase-locked to the troughs of ITDs. As time progresses, the ISWs become the dominant signature, instead of ITDs. This evolution is demonstrated in non-hydrostatic model predictions with tidal forcing by Warn-Varnas et al. (2010). Comparisons of sea surface height predictions by the hydrostatic LZSNFS model indicate that the location of ITDs tends to agree with MODIS satellite imagery and ship observations (e.g., Chao et al. 2007).

Statistical analysis of multi-year SAR data indicates that ISWs occur in SCS in April and tend not to occur in wintertime (Zheng et al. 2007). Based on the analysis of a two-layer model simulation for a shoaling thermocline with an initial solitary wave disturbance, Zheng et al. (2007, 2008) derived the internal soliton growth rate. For westward propagating ISWs in the SCS, the amplitude growth rate is positive, with maximum amplitude for summer and minimum amplitude for winter. For eastward propagation from Luzon Strait, ISWs have a negative growth rate; this explains why no ISWs are observed east of Luzon Strait. Our study is concerned with internal tide mechanism that generated westward propagating ITs, and is restricted to spring of April 2007.

In situ mooring observations also show the presence of ISWs in the SCS (Ramp et al. 2004, 2010; Farmer et al. 2009). From deployed mooring arrays, trans-basin ISWs generated at islands in the Luzon Strait region are observed (Farmer et al. 2011). These waves propagate westward and have dynamic height and isotherm displacement signatures.

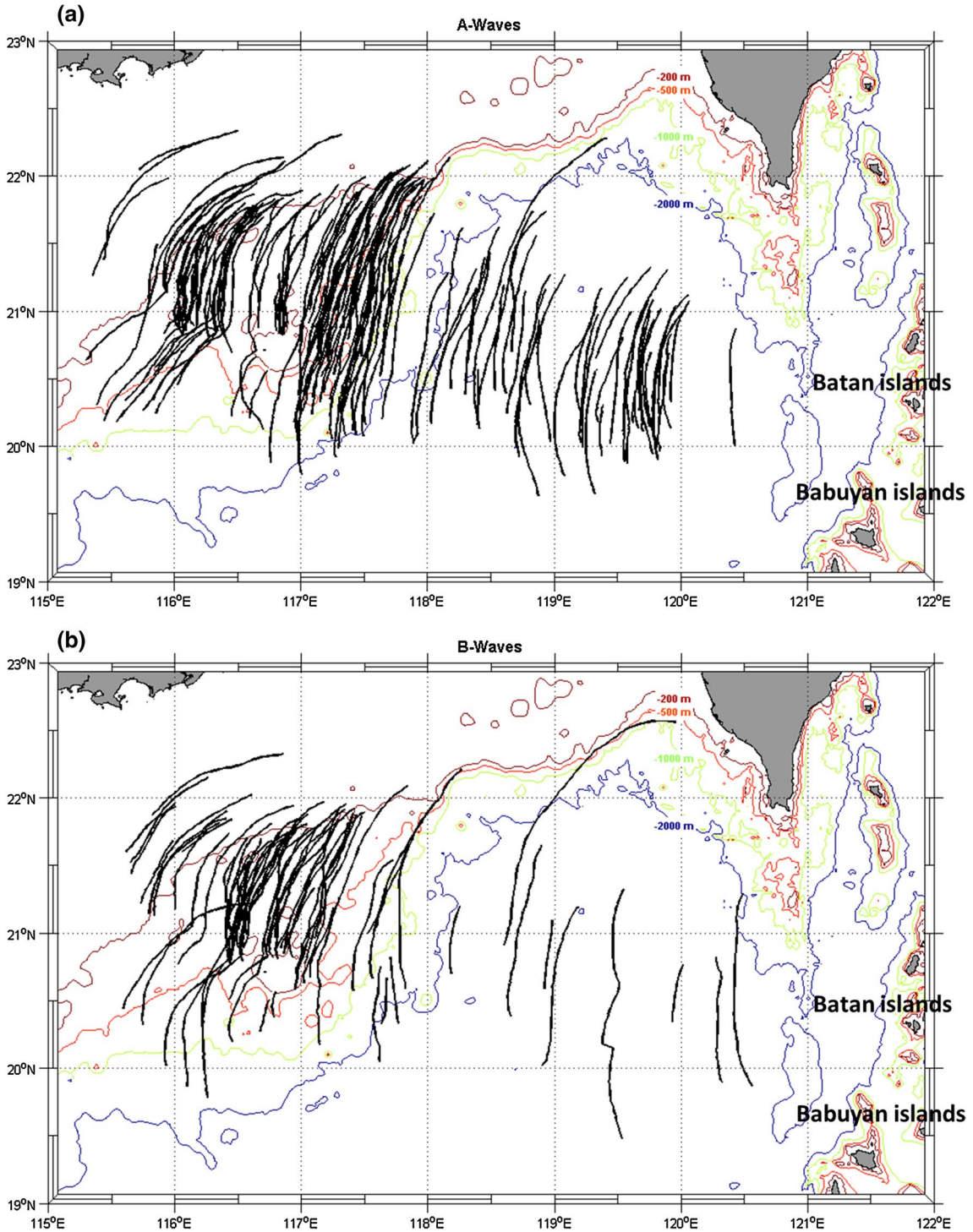

Fig. 1 **a** Location of A-waves from SAR images in the South China Sea compiled from April 2003 through December 2006; **b** location of B-waves for the same period

3 Nonlinear hydrostatic model prediction of merging IT waves

A set of predictions was conducted for April 2007 with high-resolution LZSNFS that covers the Luzon Strait, the northern South China Sea and part of the western North Pacific Ocean (Fig. 2). LZSNFS uses nonlinear hydrostatic NCOM for prediction and with realistic stratification, as described in Appendix 1. Here we applied the 2007 predictions from LZSNFS to study what an operational-type

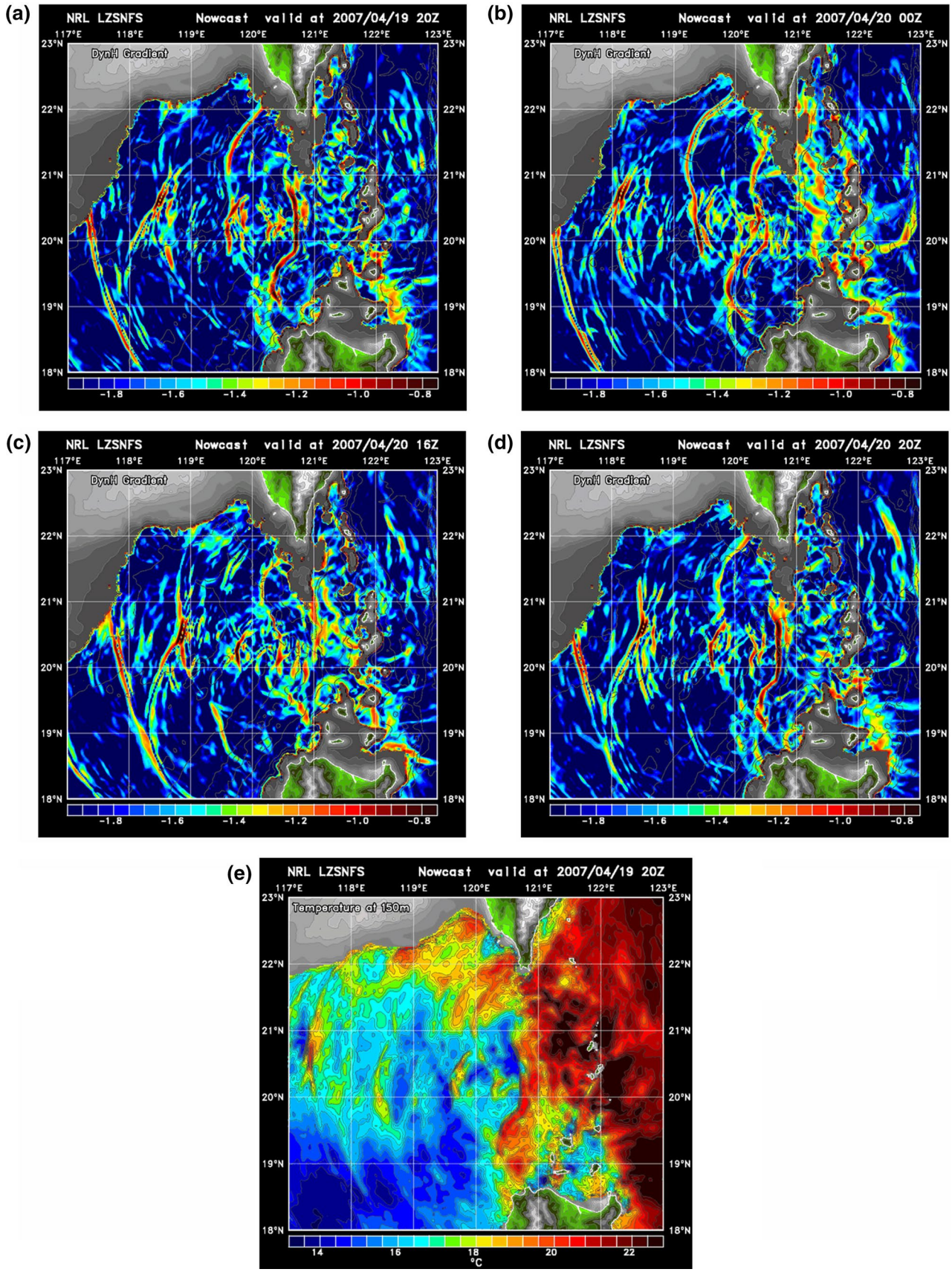
(a)
NRL LZSNFS Nowcast valid at 2007/04/19 20Z
DynH Gradient
(b)
NRL LZSNFS Nowcast valid at 2007/04/20 00Z
DynH Gradient
(c)
NRL LZSNFS Nowcast valid at 2007/04/20 16Z
DynH Gradient
(d)
NRL LZSNFS Nowcast valid at 2007/04/20 20Z
DynH Gradient
(e)
NRL LZSNFS Nowcast valid at 2007/04/19 20Z
Temperature at 150m
°C

◀ **Fig. 2** 2007 predictions of dynamic height (DH) gradients associated with ITDs: **a** 19 April, 2000 UTC, **b** 20 April 20, 0000 UTC, **c** 20 April, 1600 UTC, **d** 20 April, 2000 UTC, **e** temperature prediction at 150 m depth for 19 April 2007, 2000 UTC

forecasting system predicts for IT signatures in the SCS and Luzon Strait region. From these predictions, we track the structure of dynamic height, defined as:

$$\xi_{\mathrm{d}} = \int \frac{(\rho_{\mathrm{r}} - \rho)}{\rho_0} \mathrm{dz}$$

where ξ_{d} is dynamic height, ρ_{r} initial density, ρ predicted density and ρ_0 a constant density set to 1,025 kg/m^3. In particular, consider the horizontal gradients,

$$\nabla\xi_d = \frac{\partial\xi_d}{\partial x} + \frac{\partial\xi_d}{\partial y}$$

In actual calculation the absolute value of each derivative will be taken and the larger of the two will be plotted to base 10 logarithms (e.g., Fig. 2). A calculation of $\nabla\xi_d$ for 2000 UTC 19 April, 2007 prediction is shown in Fig. 2a. In the Luzon Strait, internal tide has a complex structure generated by the barotropic tide interacting with topography in the presence of stratification. The horizontal dynamic height gradients have a segment-like structure that varies with mesoscale and tidal variability. Some of this is also visible in other areas of the South China Sea. Westward, just outside Luzon Strait, there is a strong north–south dynamic height gradient consisting of a segment shaped with an arc and straight part. The arc tracks an internal tide depression originated from the Babuyan Inlands. The straight part tracks an ITD from the Batan Inlands. The two ITDs have combined into the shaped segment. To the right and left, there are smaller line segments generated by local interaction of barotropic tides over topography. Further west, the arcs represent local and propagating ITDs.

Four hours later, at 0000 UTC 20 April, 2007, the gradient structures have evolved into the configuration shown in Fig. 2b. The previous combined segment has moved to the vicinity of 120°E. It has evolved to a two-arc structure, from about 19°N to 21.5°N. Interactions with local topography produced structures on either side or in-between the two arcs. The previous v-shaped structure located west 119.5°E and 20.5°N has formed a line segment and combined with the arc structure above it. Sixteen hours later, at 1600 UTC 20 April, 2007, the previous structure has moved past 119°E and evolved to the configuration shown in Fig. 2c. From 119°E to 121°E, there are locally generated line segments. Twenty-four hours later, at 2000 UTC 20 April, 2007, shown in Fig. 2d, there is a similar structure (with some minor modification) to the earlier configuration shown in Fig. 2a. The predicted effects of the barotropic tide interaction with topography in presence of stratification are more or less repetitive.

The temperature at depth also exhibits ITD signatures. At 2000 UTC April 19, 2007, the temperature structure at 150 m depth has the configuration shown in Fig. 2e. There is an arc-shaped warm region between 120°/121°E and 19°/20°N that connects to a line-shaped warm region above. These warm segments correspond to dynamic height signatures in Fig. 2a and represent warm water brought down by depression ITDs. Further west, there are other ITDs propagating toward China with signatures of warm segments.

Figure 2 contains line and arc segments due to traveling ITDs and locally generated signatures by the internal waves. The length of line and arc segments is modulated by nonlinear dynamics containing mesoscale variability. The traveling ITDs predicted by LZNSFS have been compared with MODIS satellite imagery and were found to agree with the general location of ITDs that contain embedded ISWs (Chao et al. 2007). The line and arc segments of Fig. 2 exhibit similar distributions to the sketch in the Atlas of Fig. 1a and b for ISWs locations from multi-year SAR images.

In the Luzon Strait region, the mesoscale variability is dominated by the Kuroshio. Besides this variability, a cyclic intrusion of warm water southwest off Taiwan from the Pacific side often occurs. Both of these variations may influence the evolution of ITDs through nonlinear dynamics in the presence of tidal forcing (e.g., Ma et al. 2013). Figure 3, with a daily average temperature and currents at 250 m from LZSNFS, illustrates this for 19 April, 2007. The Kuroshio enters the Luzon Strait from the right side of the Babuyan Islands, flows westward of the Batan Islands, and then turns northeast to exit the strait. It separates colder

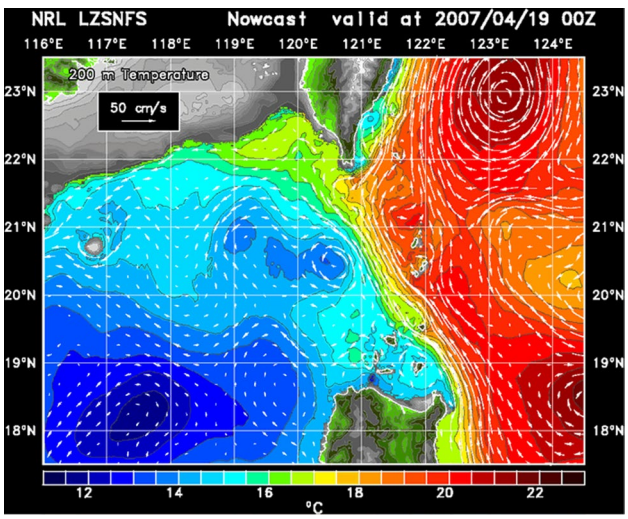

Fig. 3 The LZSNFS predicted detided daily average ocean currents and temperature at 200 m on 19 April 2007

water on the western side of the SCS from warmer water on the eastern Pacific side. There is mesoscale activity with eddies forming on both sides. The current is strong, with velocities in the order of ~1 m/s, and constitutes a frontal structure in the Luzon Strait. The back and forth movements of the barotropic tide over two sill structures of the Luzon Strait lifts the stratification up and down, generating baroclinic internal tides with depression waves propagating westward toward China and eastward toward the Pacific. These waves bring warmer water down and have a signature in barotropic and baroclinic surface elevation.

Movements of internal tide generate an internal tide energy flux: $F = \int < p'u' > dz$. The vertical integrated internal tidal energy flux averaged from 19 April to 5 May, 2007 is shown in Fig. 4. To the left of Luzon Strait, the direction of the time-averaged flux is westward. To the right, it is eastward. Out of Luzon Strait toward SCS there are northwest and southwest components that turn toward the center. In the center of SCS, there is a pronounced concentration of westward fluxes. Past 119°E, the fluxes separate into a southwest component and another that goes on turning northwest. In the Luzon Strait, the structure of energy flux is modulated by the Batan and Babuyan Islands. Fluxes from Batan and Babuyan Islands eventually join together in the center of the SCS.

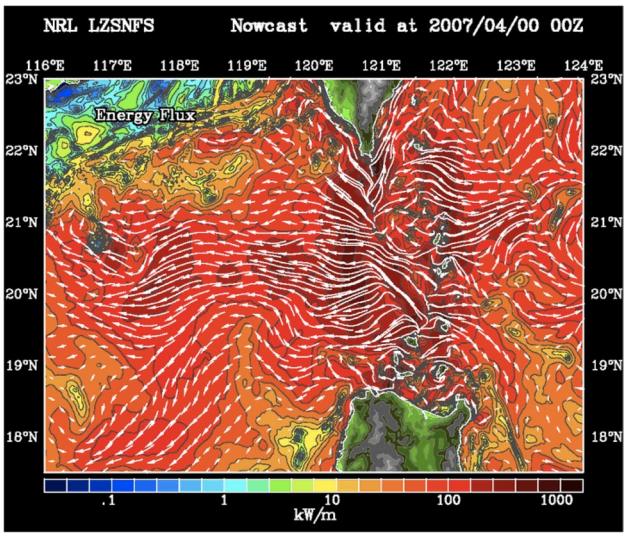

Fig. 4 Vertical integrated internal tidal energy flux averaged over 360 h from 4 April 2007 to 5 May 2007

We analyzed the effects of tidally induced dynamic variability as the internal tide waves emerge from the Batan and Babuyan Islands generation sites, by examining time series at locations close to the island chains. Close to the source sites, the dynamic height and temperature variability is due to internal tides originating at an island before interference from two generation sites occurs.

We examined LZSNFS predictions at two locations west of the Batan and Babuyan Islands, one at 121ºE and 19.3°N and the other at 121ºE and 20.5°N. Histograms of the barotropic tide, dynamic height and depth of the 18 °C isotherm at these locations over a period of 15 days are shown in Figs. 5 and 6. The locations are just outside Luzon Strait. The emphasis is on tracking internal tidal effects. The LZSNFS that applies the hydrostatic NCOM model does not represent disintegration of internal tides into internal solitary waves, nor the resultant A-waves and B-waves. It does, however, show the location of A-waves and B-waves that occur at locations of ITD.

Initially, both Figs. 5 and 6 show a strong diurnal barotropic tide and a weaker semidiurnal tide. Later in

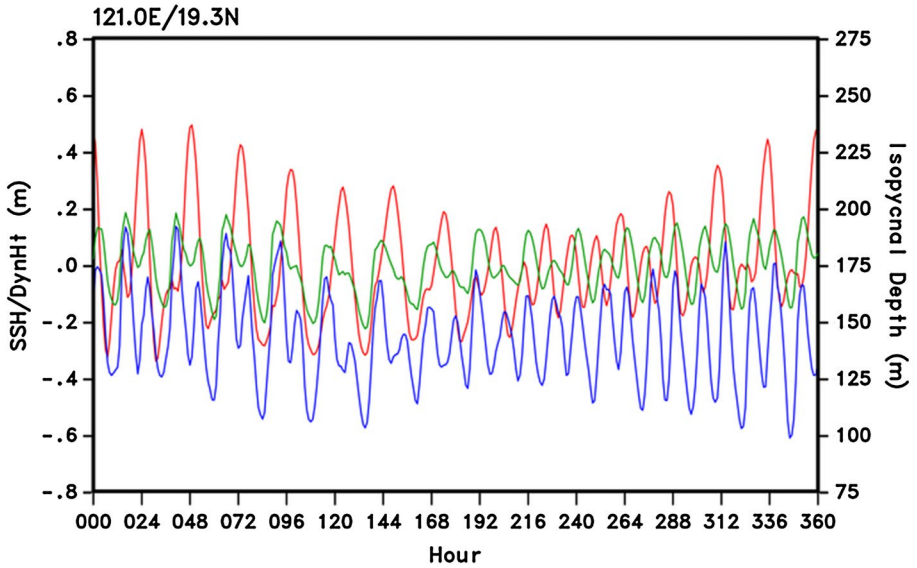

Fig. 5 LZSNFS-simulated histogram located at 121°E and 19.3°N. *Red line* for barotropic tide, *green line* baroclinic dynamic height, *blue line* 18 °C isotherm depth

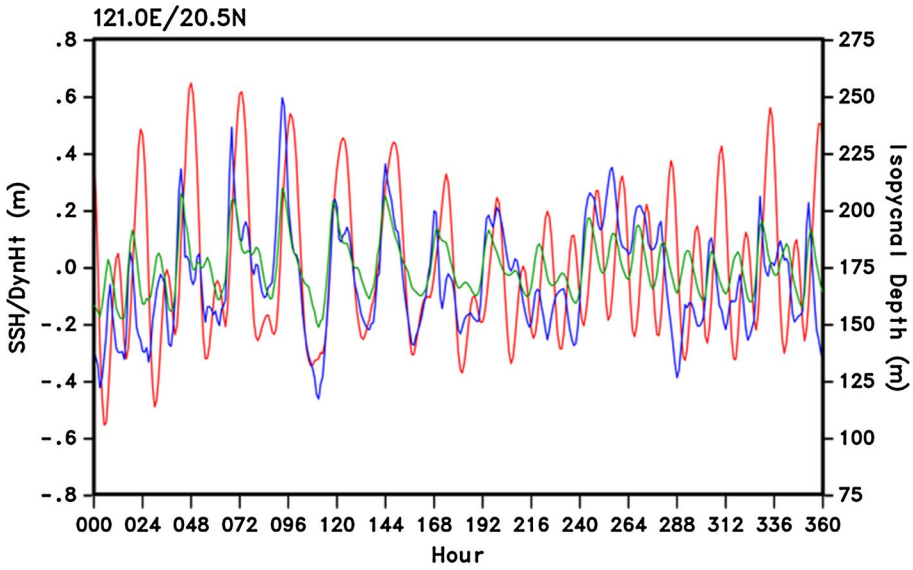

Fig. 6 The same as for Fig. 5, but at 121°E and 20.5°N

Table 1 Knife-Edge model parameters

	Center	Arc at	Arc length (km)	Direction	Radius (km)	Swat	Elevation (m)		Phase (rad)	
	x_0, y_0	x_α, y_α	α_0	θ_d	r_0	$\theta_d \pm \frac{\alpha_0}{r_0}$	ξ_{0K1}	ξ_{0M2}	ξ_{0K1}	ξ_{0M2}
Babuyan (A)	123ºE, 19.3ºN	122ºE, 19.3ºN	167	268°	110	2.93 ± .85	0.20	0.130	2.76	4.71
Batan (B)	123ºE, 20.5ºN	122ºE, 20.5ºN	167	283°	110	3.35 ± 1.07	0.15	0.034	2.76	4.71

the fortnight cycle, at about 264 h, the semidiurnal tide becomes larger than the diurnal tide. Both tidal components exhibit the fortnight cycle with a minimum at about 216 h. The dynamic height and 18 °C isotherm responses are shifted in time relative to the barotropic velocity. At 120ºE and 19.3°N, the dynamic height and 18 °C isotherm exhibit the fortnight effect with an increase in semidiurnal magnitude relative to diurnal after fortnight minimum. At 121ºE and 20.5°N, the fortnight minimum trend and the magnitude dominance from diurnal to semidiurnal occur for barotropic tide. Dynamic height and 18 °C isotherm exhibit the fortnight effect with an increase in semidiurnal magnitude relative to diurnal magnitude after the fortnight minimum. There are, however, phase shifts after the fortnight minimum due to dynamic evolution. In particular, after the fortnight, the variation of the envelop structure in Fig. 6 is influenced by an eddy at the left of the location and meanders of the Kuroshio front, shown in Fig. 3.

4 Interference patterns of IT waves predicted with a linear knife-edge model

Hydrostatic model predictions, SAR observations, and in situ data suggest ITD generation sites at the Batan and Babuyan Islands. The generated ITD propagates westward and northwestward with surface elevation signature. An internal tidal depression propagates as a wave; two such ITDs from two different sources can cause an interference pattern. Such interference patterns have been observed during the Hawaiian Oceans Mixing Experiment (HOME) and associated hydrostatic model predictions (Rainville et al. 2010).

The waves from line sources can cause interference patterns. Further away from sources, the interference patterns form arcs of a circle. Such arcs are similar to what is seen in Fig. 2. ITDs surface elevation signatures can also be represented with a knife-edge model of St. Laurent et al. (2003); see Appendix 2 for a description of the knife-edge model. This model represents an ITD wave propagating in a plane from sources on a line with the path confined to an angular segment area or swat. The knife-edge model was shown by Rainville et al. (2010) to reproduce the main interference features of ITDs surface elevation signatures observed during HOME.

Consider internal tides generated by K_1 and M_2 components at the Batan and Babuyan Islands. Relative to the islands, the ITDs propagate in the horizontal at an angle. The deduced angles from ASIAEX data analysis by Ramp et al. (2004; 2010) are 282° from the true north

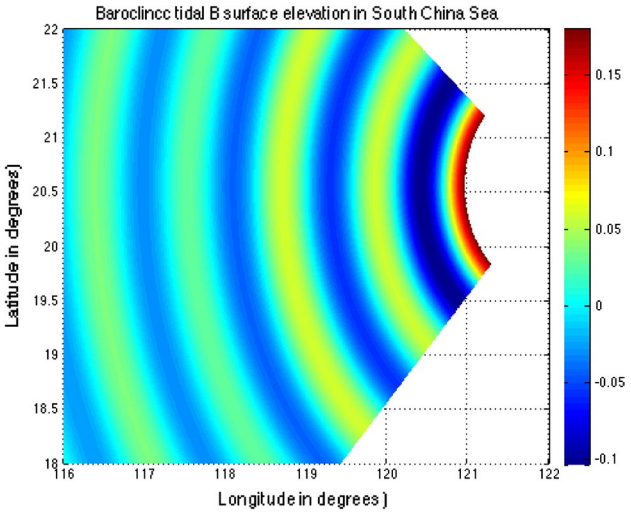

Fig. 7 Dynamic height elevation from source at Batan Islands

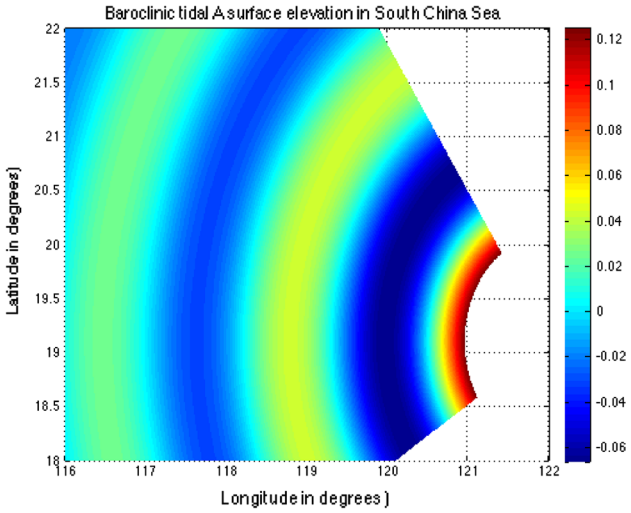

Fig. 9 Dynamic height elevation from the source at the Babuyan Islands with K_1 component

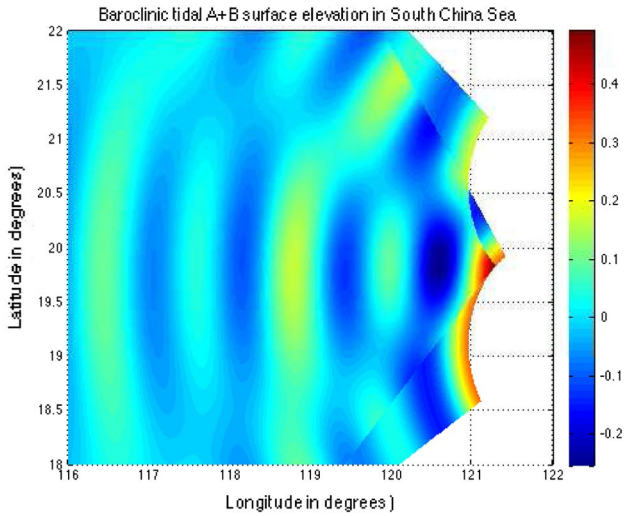

Fig. 8 Interference pattern of dynamic height elevation from K_1 and M_2 tides originating at Batan and Babuyan Island sources

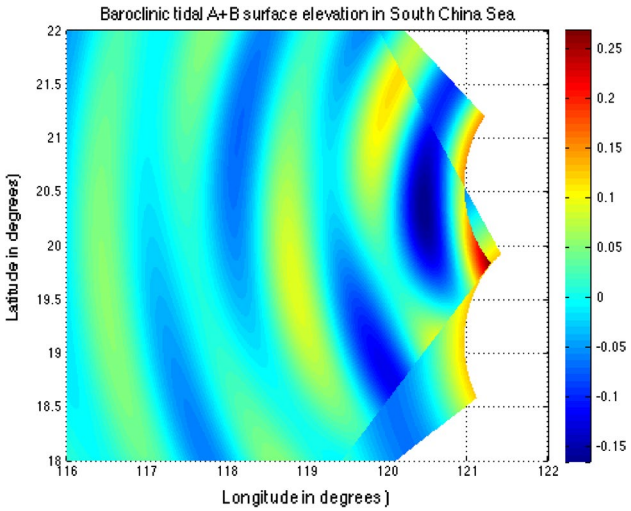

Fig. 10 Dynamic height elevation from the source at the Batan Islands with M_2 component, and with K_1 component at the Babuyan Islands

at the Babuyan Islands and 267° at the Batan Islands. We assumed line sources for the islands; with an extent of 167 km for both the Batan chain and the Babuyan chain. Line sources are on a vertical line along 122°E. An angular span or swat is assigned to the line sources in cylindrical coordinates, with the origin to the right of 122°E, at 123°E (Table 1). The centering of the swats are 282° for the Babuyan Islands and 267° for the Batan Islands.

Using the parameters of Table 1, baroclinic surface elevation patterns were calculated over an angular spread or swat in cylindrical coordinates. Outside the swat, surface elevation was set to zero. Figure 7 shows the K_1, M_2 baroclinic surface elevation distributions arising from the Batan Islands in cylindrical coordinates. Each of the swats consists of circular positive and negative elevation centered at the cylindrical coordinate origin. The patterns are circular around the origin and contain the signatures of diurnal (K_1) and semidiurnal (M_2) wavelengths. Figure 8 is a superposition of K_1 and M_2 tides, both originating at the Batan and Babuyan Islands. Tides and phase were extracted from Oregon State University (OSU) tidal database (Egbert and Erofeeva 2002), and are listed in Table 1. We did some simulations with zero phase and obtained similar results.

Over the superposition region, the patterns are no longer circular. They form arcs of negative and positive elevations. The arc region forms a swat with shifted nodal lines

on each side. The arcs are generated through interference of waves from the Babuyan and Batan Islands. The arc lengths increase with distance from the sources. Such arcs are seen in SAR images. The arcs suggest an interference mechanism of internal tidal depressions propagating from the Batan and Babuyan Island regions. The ITDs bring warm water down and when the ITDs merge through interference, they exhibit warm water arcs in the horizontal, as in Fig. 2e.

Assume IT generation to be K_1 at the Babuyan Islands and M_2 at the Batan Islands. The K_1 patterns from Babuyan are shown in Fig. 9. The K_1 diurnal tide exhibits the larger wavelength (~240 km) compared to the M_2 semidiurnal tide (~120 km). The superposition of M_2 tides from the Batan Islands and K_1 tides from the Babuyan Islands produces the interference patterns shown in Fig. 10. The line spacing in the interference swat suggests semidiurnal wavelength dominance. The structure of the patterns contains shifting arc location and length along radial distance. Inside the structure of the pattern, there are suggestive repetitions of shifted arc segments. The K_1 diurnal internal tide acts as a modulator of the M_2 semidiurnal tide. Some mooring measurements suggest that ITDs arriving from Babuyan Inlands tend to be K_1 waves, and those from Batan, M_2 waves (Ramp et al. 2004, 2010).

5 Discussion

Modeling studies of SCS internal waves show that ITs are generated at the Batan and Babuyan island chains (e.g., Zhang et al. 2011). From resultant ITDs, disintegration into both A-waves and B-waves develops in the SCS. The double ridge Luzon Strait structure that encompasses the island chains exerts an influence on IT wave generation. In the northern region of Luzon Strait, bottom topography slope is critical and results in internal tidal energy beams that amplify IT waves as they propagate westwards. The spacing between the eastern and western ridges is about one semidiurnal tidal wavelength and leads to resonance with the semidiurnal tide that amplifies IT waves (Warn-Varnas et al. 2010; Zhang et al. 2011).

In the southern region of Luzon Strait, critical topography slope also results in energy beams that amplify IT waves as they propagate westward. Tracking of ITDs and the subsequent evolved ISWs indicates two directions of wave propagation at 282° and 267°. The 282° direction tracks waves from the Batan Islands and 267° tracks waves from the Babuyan Islands, as shown by Ramp et al. (2010).

The influence of the two-ridge LS configuration on the generation and propagation of ISWs is being researched. The roles of western and eastern ridges at LS are of particular interest. Chao et al. (2007) show that in an idealized double-ridge topography of LS, increase of the western ridge height leads to damping of ISWs and a decrease leads to amplification of ISWs. Echeverri et al. (2011) demonstrate that in a double ridge system, internal-wave rays can be trapped, forming internal tide attractors. Li and Farmer (2011) studied the generation and evolution of nonlinear internal waves (IWs) in LS and SCS. They found that the amplitude of IWs is related more to the amplitude of the semidiurnal tide than to the dominant diurnal tide. They showed that LS ridge separation of about one semidiurnal tidal wave length leads to intensification of the westward propagating semidiurnal tide. They also demonstrated that westward intrusion of the Kuroshio tends to suppress nonlinear wave generation. Buijsman et al. (2012) studied double-ridge internal tide interference in LS. They established that for semidiurnal barotropic tides, the internal wave beams in the double ridge LS structure almost superpose after one surface reflection. This leads to stronger barotropic to baroclinic energy conversion and dissipation, as compared to a single ridge. Li (2014) performed an assessment of factors affecting nonlinear ITs in SCS. The study focused on nonlinear ray interaction between western and eastern LS ridges. For semidiurnal tide, the western ridge intensifies in-phase ray interaction with the semidiurnal tide generated at the eastern ridge. For diurnal tide, an antiphase ray interaction occurs and diurnal tide generation is reduced. His model simulations show that westwards flow of Kuroshio (that tends to occur in winter) reduces amplitude of internal tides in SCS, and that winter stratification cannot account for a reduction of ISWs.

Buijsman et al. (2010) performed a two-dimensional, nonhydrostatic modeling study of east–west asymmetry of nonlinear ISWs in LS. They considered the effects of thermocline depth variations, bathymetry, Kuroshio current, rotation, internal tide resonance in LS double ridge, and a deep Pacific Ocean. Results indicated that on the east side of LS, ISWs are smaller than on the west side, due to an asymmetric modulated barotropic tide at the east ridge of LS. Also, a dispersion analysis of ITs into ISWs showed that ISW growth is larger on the west side of LS where the thermocline is more shallow (shoaling), than on the east Pacific Ocean side where thermocline is deep. This trend agrees with satellite imagery that indicates westward ISWs are more numerous than eastward ISWs.

Li (2014) also assessed the effects of double-ridge topography, stratification, rotation, Kuroshio, and tides applying the MITgcm. Results indicated that diurnal internal tide generation is suppressed by rotational effects, and that the double ridge configuration in LS reduces the internal diurnal tide and reinforces the semidiurnal tide. He showed that the Kuroshio suppresses the evolution of ITs east of LS and that ITs decay as they propagate eastward along a deepening thermocline. As a result, fewer ISWs develop on the Pacific Ocean side. Under the effects of nonlinearity, rotation, and nonhydrostatic dispersion, the nonlinear waves can have different kind of shapes. He found that seasonal

westward inflow of Kuroshio into SCS reduces amplitude of ITs in the SCS, and consequently ISWs. This contributes to fewer solitons in SCS during the winter.

In the nonlinear hydrostatic model predictions, the ITDs have signatures in surface elevation, dynamic height gradients, temperature and velocity. Dynamic height gradients exhibit arc segment and arc structures (Fig. 2). Due to nonlinear effects, mesoscale variability and ocean currents, there are no visible nodes at the end of the arcs, as in the case of the linear knife-edge model. In Fig. 2a, two joined ITD waves have emerged from Luzon Strait. They combined into a structure of an arc and a segment. As the combined structure propagates westward, it tends to become more circular and elongated (Fig. 2b) before shoaling onto the Chinese continental shelf (Fig. 2c). Images of SAR observation in the SCS indicate arcs on west side of the Batan and Babuyan island chains (Liu et al. 2004). The arc surface elevation signatures propagate and merge into larger combinations of arcs that are seen in SAR data archives (Fig. 1a, b) (Jackson 2009, 2014).

Taking the Batan and Babuyan Islands as sources of ITDs, application of the linear knife-edge model enables calculating interference patterns in a basic superposition sense. Such a calculation yields interference patterns as shown in Fig. 8. The patterns consist of arcs with positive and negative elevations separated by nodes with shifts past the nodes. The arcs enlarge with distance away from the two sources at Luzon Strait. The enlargement of the arcs and shift after the nodes is similar to what is seen in a nonlinear hydrostatic model (Fig. 2). There are, however, no ocean dynamics, nor is there lateral viscosity in the linear knife-edge model. Currents, eddies, topography and dissipation effects that influence the shape of the merged wave arc signatures are also neglected in the knife-edge model.

A point of interest is assuming that the tidal generation at the Batan Islands to be M_2 dominant and at the Babuyan Islands to be K_1 dominant. Some of the data analysis from observation suggests such dominance (e.g., Ramp et al. 2004, 2010; Zhang et al. 2010). This, however, is not to suggest that the other tidal components are not present. With this assumption, there is a shift in interference pattern (Fig. 10). The structure now has positive and negative elevation arcs with their own respective nodes. The arcs are interspaced with changing directionality relative to sources. This suggests another level of complexity that can be encountered in data analysis.

6 Conclusion

Predictions with the nonlinear hydrostatic LZSNFS indicate generation of IT waves at the Batan and Babuyan Islands, propagation westward and subsequent merging in the SCS. The merged IT waves form arc segment patterns of surface elevation that elongate in the north-south direction as the waves propagate farther westward and eventually shoal on Chinese continental shelf. The IT waves have a signature throughout the water column in terms of temperature, salinity, and velocity. Warm water is brought down by IT depressions, forming warm spots at depths where IT waves are located.

We investigated merging of IT waves with a basic linear superposition approach by considering two sources of IT waves. We adapted and applied the linear knife-edge model of baroclinic tides that originate at the Batan and Babuyan Islands. Results showed an arc-type interference pattern with shifts at the nodal ends. Arc lengths increased with distance from the sources, similar to SAR observations. Assuming a K_1 tidal wave from the Babuyan Islands and an M_2 tidal wave from the Batan Islands, the model indicated a K_1 modulation of interference patterns with an angular shifting of arcs relative to each other.

Arc type interference patterns occur in the nonlinear hydrostatic model and the linear wave superposition model of the SCS. The nonlinear hydrostatic model contains mesoscale variability with Kuroshio at Luzon Strait. Their effects result in increasing arc lengths from Luzon Strait without nodes at the ends of the merged arcs. Increasing arc lengths are similar to interference from the linear wave superposition obtained with the knife-edge model. The phenomenon of interference from two sources is predicted by the nonlinear hydrostatic model.

The model-predicted horizontal gradient exhibited ITDs and mesoscale variability signatures. Satellite SAR observations contain signatures of ITDs and internal solitary waves, into which ITDs disintegrate as amplitude and frequency dispersion set in. Merging of ITDs from the Batan and Babuyan Islands is observed in model predictions and SAR observations. The merged arc structures propagate west and northwest, become more circular and increase in length. On the Chinese continental shelf, the ITDs waves shoal and there are more ITDs appearing through fission and local generation. This is visible in SAR observations and model predictions.

Acknowledgments The work was supported by the Office of Naval Research under PE62435N for AWV and N00014-05WX-2-0647 for DSK, with technical management provided by the Naval Research Laboratory. We thank Gretchen Dawson and Paul Martin for the early NCOM predictions and analysis. Helpful comments from two anonymous reviewers are appreciated.

Appendix 1: Hydrostatic model (LZSNFS)

The LZSNFS (Luzon Strait Nowcast/Forecast System) is an integration of a data-assimilating, dynamical ocean

model, a statistical data-analysis model, and various data streams for ocean bathymetry, climatological data, surface forcing, open boundary forcing, and observations for data assimilation (Ko et al. 2008). The dynamic ocean model in the system is the Navy Coastal Ocean Model (NCOM) (Martin 2000), developed at Naval Research Laboratory (NRL) and in operation at the US Naval Oceanographic Office in various configurations (Rhodes et al. 2002). NCOM is a hybrid sigma/z-level primitive equation, free-surface model, applying the hydrostatic, incompressible, and Boussinesq approximations. This model is similar in its physics and numeric to the Princeton Ocean Model (POM), but uses an implicit treatment of the free surface.

The LZSNFS model domain covers the Luzon Strait, northern South China Sea and part of the western North Pacific Ocean (Fig. 3) with ~2.3 km horizontal resolution. There are 41 sigma-z levels in the model; 19 sigma layers are used from the surface down to a depth of 147 m, and z-levels are used below. The model ocean topography is derived from the NRL global Digital Bathymetry Data Base 2-min (DBDB2) (http://www7320.nrlssc.navy.mil/DBDB2_WWW/), with improvement by blending high resolution bathymetry data from the Ocean Research Center at National Taiwan University.

The LZSNFS applies the East Asian Seas Nowcast/Forecast System (EASNFS; Ko et al. 2009; Lee et al. 2013; Ko et al. 2014) that covers entire East Asian Marginal Seas for open boundary conditions (BCs). The EASNFS for this application does not include tides. To simulate internal tides/waves, LZSNFS are forced with tidal heights and transport of eight tidal harmonics (K_1, O_1, P_1, Q_1, M_2, S_2, K_2, and N_2) taken from TPXO7.2 (Egbert and Erofeeva 2002). Tides are applied to model depth-averaged normal velocity u, with elevation η, at open boundary by combining forcing from EASNFS using a forced radiation BC modified from Flather and Proctor (1983):

$$u = (u_R + u_t) \pm c[(\eta_R + \eta_t) - \eta]/h,$$

where subscript R and t denote variables from the regional model (EASNFS) and from the tidal model, respectively, and c is the barotropic wave phase speed: $c = \sqrt{gh}$, with g being the gravitational constant and h the water depth. For the BCs of tangential velocity, temperature and salinity, the first-order-upwind advection scheme was utilized.

The atmospheric forcing consists of air pressure, wind stress, solar radiation, and heat fluxes from Coupled Ocean/Atmosphere Mesoscale Prediction System (COAMPS), a high-resolution Navy operational regional weather forecast model.

LZSNFS assimilates satellite altimeter data to produce Kuroshio and mesoscale eddies that have been shown to have an impact on the generation and propagation of large amplitude internal waves (e.g., Ma et al. 2013). A vertical weighting function and a scale separation scheme are applied for the data assimilation to prevent attenuation of high frequency internal tides/waves (Chen et al. 2013; Ko and Wang 2014).

Appendix 2: Knife-edge model

The knife-edge model represents the baroclinic surface elevation in cylindrical coordinates as:

$$\varsigma(t, r, \theta) = \varsigma_0 \left(\frac{r_0}{r}\right)^{1/2} \exp(i\vec{k}_r . \vec{r} - \mathrm{iwt} + \phi_0) \quad for\ |\theta - \theta_0| < a_0/2\, r_0,$$

where r is the distance from the center, ς_0 amplitude of baroclinic surface elevation at r_0 and ϕ_0 arbitrary phase. Equation evaluated for $r > r_0$ Wave is evaluated for $r > r_0$. Wave is prevented from radiating in all directions by assigning length a_0, direction $_0$ with range $\theta_0 \pm (a_0/2r_0)$, and $\varsigma = 0$ elswhere.

A ridge where generation occurs can be represented by a line source. Generation from several ridges can be superposed with this knife edge model. Propagation angle is established by the strongest barotropic tidal current direction. The phase is chosen for baroclinc currents to have the same phase as the maximum cross ridge barotropic tide. The wavelengths are calculated based on stratification used in model. The surface elevation is determined for the generated wave at the line source to carry the energy across the channel predicted by the knife-edge model (Rainville et al. 2010). Phases ϕ_0 are derived from the OSU (University of Oregon) tidal model.

References

Buijsman MC, McWilliams JC, Jackson CR (2010) East-west asymmetry in nonlinear internal waves from Luzon Strait. J Geophys Res 115:C10057. doi:10.1029/2009JC006004

Buijsman M, Legg S, Klymak J (2012) Double ridge internal tide interference and its effect on dissipation in Luzon Strait. J Phys Oceanogr 42:1337–1356

Chao S-Y, Ko DS, Lien R-C, Shaw P-T (2007) Assessing the west ridge of Luzon Strait as an internal wave mediator. J Oceanogr 63:897–911. doi:10.1007/s10872-007-0076-8

Chen Y-J, Ko DS, Shaw P-T (2013) The generation and propagation of internal solitary waves in the South China Sea. J Geophys Res 118:6578–6589. doi:10.1002/2013JC009319

Echeverri P, Yokossi T, Balmforth NJ, Peacook T (2011) Tidally generated internal-wave attractors between double ridges. J Fluid Mech 669:354–374

Egbert G, Erofeeva S (2002) Efficient inverse modeling of barotropic ocean tides. J Atmos Ocean Tech 19:183–204

Farmer D, Li O, Park J-H (2009) Internal wave observation in South China Sea: the role of rotation and nonlinearity. Atmos-Ocean 47:267–280. doi:10.3137/OC313.2009

Farmer DM, Alford MH, Lien R-C, Yang Y-H, Chang M-H, Li Q (2011) Stages in the life of an internal wave. Oceanography 24:64–77

Flather RA, Proctor R (1983) Prediction of North Sea storm surges using numerical models: recent developments in the UK. In: Sundermann J, Lenz W (eds) North Sea dynamics. Springer, New York, pp 299–317

Hsu M, Liu A (2000) Nonlinear internal waves in South China Sea. Can J Remote Sensing 26:72–81

Jackson CR (2009) An empirical model for estimating the geographic location of nonlinear internal solitary waves. J Atmos Oceanic Technol 26:2243–2255. doi:10.1175/2009JTECHO6381

Jackson CR (2014) Separation of SAR observations into A and B waves. Private communication

Ko DS, Wang D-P (2014) Intra-Americas Sea nowcast/Forecast System Ocean reanalysis to support improvement of oil-spill risk analysis in the gulf of Mexico by multi-model approach, BOEM 2014-1003. Bureau of Ocean Energy Management, Herndon, VA, pp 55

Ko DS, Martin PJ, Rowley CD, Preller RH (2008) A real-time coastal ocean prediction experiment for MREA04. J Mar Syst 69:17–28. doi:10.1016/j.jmarsys.2007.02.022

Ko DS, Chao S-Y, Huang P, Lin SF (2009) Anomalous upwelling in Nan Wan: July 2008. Terr Atmos Ocean Sci 20:839–852. doi:10.3319/TAO.2008.11.25.01(Oc)

Ko DS, Chao S-Y, Wu C-C, Lin I-I (2014) Impacts of Typhoon Megi (2010) on the South China Sea. J Geophys Res Oceans 119:4474–4489. doi:10.1002/2013JC009785

Laurant LC, Stringer S, Garret C, Perrault-Joncas D (2003) The generation of internal tides at abrupt topography. Deep Sea Res I 50:987–1003

Lee I-H, Ko DS, Wang Y-H, Centurioni L, Wang D-P (2013) The mesoscale eddies and Kuroshio transport in the western North Pacific east of Taiwan from 8-year (2003–2010) model reanalysis. Ocean Dyn 63:1027–1040. doi:10.1007/s10236-013-0643-z

Li Q (2014) Numerical assessment of factors affecting nonlinear internal waves in South China Sea. Prog Oceanogr 121:24–43

Li Q, Farmer DM (2011) The generation and evolution of nonlinear internal waves in the deep basin of the South China Sea. J Phys Oceanogr 41:1345–1363

Liu A, Ramp S, Zhao Y, Tang Y (2004) A case study of internal solitary wave propagation during ASIAEX 2001. IEEE J Ocean Eng 29:1144–1156

Ma BB, Lien R-C, Ko DS (2013) The variability of internal tide in the northern South China Sea. J Oceanogr 69:619–630. doi:10.1007/s10872-013-0198-0

Martin PJ (2000) A description of the Navy Coastal Ocean Model Version 1.0, NRL. Rep. NRL/FR/7322-00-9962. Nav Res Lab Stennis Space Cent., MS, pp 42

Niwa Y, Hibiya T (2004) Three-dimensional numerical simulation of M2 internal tides in the East China Sea. J Geophys Res 109:C04027. doi:10.1029/2003JC001923

Qian H, Shaw P-T, Ko DS (2010) Generation of internal waves by barotropic tidal flow over a steep ridge. Deep Sea Res I 57:1521–1531. doi:10.1016/j.dsr.2010.09.001

Rainville L, Johnston S, Carter TM, Merrifield GS, Pinkel MA, Worcaster PF, Dushhaw BD (2010) Interference pattern and propagation of the M2 internal tide south of the Hawaiian Ridge. J Phys Oceanogr 41:311–325. doi:10.1175/2009JPO4256

Ramp S, Tang T, Duda T, Lynch J, Liu A, Chiu C-S, Bahr F, Kim H-R, Yang Y-J (2004) Internal solitons in the Northeastern South China Sea Part 1: sources and deep water propagation. IEEE J Ocean Eng 29:1137–1181

Ramp S, Yang Y, Bahr F (2010) Characterizing the nonlinear internal wave climate in the northeastern South China Sea. Nonlin Proc Geophys 17:481–498. doi:10.5.5194/npg-17-481-2011

Rhodes RC, Hurlburt HE, Wallcraft AJ, Barron CN, Martin PJ, Smedstad OM, Cross S, Metzger EJ, Shriver J, Kara A, Ko DS (2002) Navy real-time global modeling system. Oceanography 15:29–43. doi:10.5670/oceanog.2002.34

Simmons H, Chang M-H, Chang Y-T, Chao S-Y, Fringer O, Jackson CR, Ko DS (2011) Modeling and prediction of internal waves in the South China Sea. Oceanography 24:88–99. doi:10.5670/oceanog.2011.97

Warn-Varnas A, Hawkins J, Lamb KG, Piacsek S, Chin-Bing S, King D, Burgos G (2010) Solitary wave generation dynamics at Luzon Strait. Ocean Model 31:9–27. doi:10.1016/j.ocemod.2009.08.002

Zhang Z, Fringer OB, Ramp S (2011) Three-dimensional nonhydrostatic numerical simulation of nonlinear internal wave generation and propagation in the South China Sea. J Geophys Res 116:C05022. doi:10.1029/2010JC006424

Zheng Q, Susanto RD, Ho C-R, Song YT, Xu Q (2007) Statistical and dynamical analyses of generation mechanisms of solitary internal waves in the northern South China Sea. J Geophys Res 112:C03021. doi:10.1029/2006JC003551

Zheng Q, Song YT, Lin H, Hu X, Meng J, Wang D (2008) On generation source sites of internal waves in the Luzon Strait. Acta Oceanol Sin 27:38–50